Triple-screw pumps for ICE cooling systems in the transportation sector

Giammarco Di Giovine[1,*], *Luigi* Mariani[1] , *Marco* Di Bartolomeo[1], *Davide* Di Battista[1], and *Roberto* Cipollone[1]

[1] Università degli Studi dell'Aquila, Dipartimento di Ingegneria Industriale e dell'Informazione e di Economia, 67100 L'Aquila, Italy

Abstract. Recent EU Regulations have been pushing the transportation sector increasingly towards the reduction of primary harmful pollutants and CO_2 emissions. In this context, the Internal Combustion Engine (ICE) cooling system is gaining a new technological interest. In fact, improvements on pump efficiency can significantly reduce its absorbed energy during real on-the-road operation. Typically, centrifugal pumps are adopted, but their efficiency is highly dependent on rotational speed, wasting energy during real operation, even if they are designed to have a very high efficiency at the design point. This study investigates the three screws pumps potentiality to substitute traditional centrifugal pumps in engine cooling applications. In fact, triple-screw pumps belong to positive displacement pumps, which have an efficiency ideally independent on rotational speed.

A zero-dimensional mathematical model of this pump previously developed by the authors was improved, giving a specific focus on the mechanical efficiency of the pump. The validation of the model resulted in a good agreement with experimental results. The model has been used to design a pump for an IVECO F1C diesel engine. The energy requested to drive the pump over a Worldwide Harmonized Light Vehicles Test Cycle (WLTC) has been calculated and compared with that of the traditional existing centrifugal pump. Results show that the electrically actuated triple screw pump allows to reduce the energy of about 14 %.

1 Introduction

During the recent years, emissions of CO_2 and primary pollutants caused by on the road transportation sector have been limited by the European Union (EU) through increasingly strict regulations [1, 2]. In fact, about 28% of the CO_2 emissions was caused by the aforementioned sector in 2019 [3].

To face this issue, vehicle manufacturers are increasing the production of hybrid and electric vehicles [4], which may help in reducing primary pollutants in urban areas [5], but hardly in reducing CO_2 emissions [6]. In fact, the LCA (Life Cycle Assessment) of BEVs (Battery Electric Vehicles) indicate that the power generation mix of a Country should keep CO_2 emissions below 320 g/kWh to produce a net benefit [7].

---

* Corresponding author: giammarco.digiovine@graduate.univaq.it

On the other hand, thermal engine vehicles still have opportunities of development, especially those regarding the engine thermal management. As known, in fact, almost 2/3 of the whole harmful emissions is produced during engine warm-up in common driving cycles [8]. During this phase, the temperatures of coolant water and lubricant oil are not at their optimal value [9, 10] able to guarantee the higher overall engine efficiency, as well as to improve the performance of aftertreatment devices, which reduce the formation of pollutants.

This issue can be solved acting on the engine cooling pump to speed up the engine warm-up phase. Moreover, the recent integration of different thermal needs in the engine cooling system (charge air cooling [11, 12, 13], air conditioning condenser [14], separated cooling between engine head and block [15], cabin heater, etc.) is functional to a suitable downsizing of the engines and enhancing the overall system efficiency; on the other hand, it produced an increased complexity, which claims for additional degrees of freedom in developing cooling strategies [16, 17, 18].

Typically, centrifugal pumps mechanically linked to the crankshaft are used to move the engine cooling fluid. This technology does not allow to vary the pump speed independently from the engine speed, preventing a high pump efficiency, which depends highly on the impeller speed. In fact, centrifugal pumps are designed at the Best Efficiency Point (BEP), located at high flow rate and rotational speed, corresponding to the maximum engine mechanical power. However, the pump operates far from the BEP during homologation cycles, resulting in a lower pump efficiency (between 15-20%), and thus in a significant power absorbed compared to the propulsion one [19]. An electrically actuated centrifugal pump would produce a faster engine warm-up, but not a pump efficiency increase.

This paper investigates the use of screw pumps as cooling pumps for automotive engines. Their use in this sector is still unexplored, even if their performances in other applications suggest good potentialities. In fact, screw pumps efficiency is substantially independent on rotational speed, as it happens for rotary volumetric pumps [20, 21]. Therefore, efficiency improvements relatively to centrifugal pumps are expected, as already observed for sliding vane pumps [22, 23].

Screw machines have been widely studied in terms of thermodynamic and fluid flow modelling when used as compressors [24] and expanders [25], and their geometry has been optimized to reduce wear and friction [26, 27]. These problems also affect screw pumps, which therefore have been studied mostly when operating with clean and lubricating fluids [28].

Screw pump performances depend strictly on the rotor profile shape [29], due to its influence on friction, and thus on wear, and on blow hole backflow. The optimization of the rotor profile can be realized by varying the blunting of the screw profile or the screw shape: in the first case [30], the volumetric efficiency of a three-screw pump was significantly improved adopting a new rotor profile with elliptic arc, which reduces the blow hole area; in the second case [31], the overall efficiency of a twin-screw oil pump was maximized, optimizing the involute meshing angle of the screws.

Screw pumps performances can be predicted also by CFD models. Advanced numerical models with many features for design have already been developed [32], capable to analyse also vacuum applications [33], as well as cavitation phenomena [34].

However, a zero-dimensional approach is pursued in this paper. In fact, contrarily to CFD methods, lumped parameters models can be used easily as a virtual platform to support design processes, being generally lighter and less computationally expensive.

Several lumped parameter models have already been developed in literature. A triple screw pump for an aerospace application has been studied in [35], where a parametric analytical model was developed and validated, adapting the boundary-layer theory [36] to calculate the volumetric performances of the pump. A trade-off between backflow and wear resistance in triple screw pumps was investigated in [37], through a detailed theoretical

model. That study was subsequently deepened in [38], where the pressure loads acting on the pump rotors were calculated, and in [39], where the dynamic effects of these loads were simulated and experimentally validated.

Lumped parameter models have been developed also for multiphase screw pumps: a twin-screw multiphase pump was studied in [40], where a complete thermodynamic model was developed and experimentally validated, and in [41] this modelling has been further improved considering gas-liquid mixtures with very high gas volume fractions (up to 99 %).

Similarly, also screw vacuum pumps have been characterized and optimized through accurate lumped parameter models: conical rotors were investigated in [42] because of their potential to enhance screw vacuum pumps performances, while a screw rotor with continuously varying cross section profiles and screw pitch has been developed in [43], demonstrating better volumetric and mechanical performances compared with the existing variable pitch screw rotor.

Using screw pumps as cooling pumps of ICEs is a new potential field of application, which suggests the identification of a specific redefined 0-D model. Engine cooling applications require reliable and cost-effective manufacturing solutions for the cooling pump, and this applies also when using screw pumps. Therefore, the triple screw pump considered in this paper adopts a simple layout, with the driver screw aligned with only one bearing, and the other two idler screws simply entrained inside a cylindrical support. This simple manufacture enables occasional dry contacts between the screws and the pump case, increasing the complexity of mechanical losses modelling.

A novel zero-dimensional mathematical model capable to predict the performances of triple-screw pumps with the afore mentioned simple layout has already been developed by the authors in [44]. The present paper offers a deeper knowledge of the mechanical efficiency of the pump, investigating the physical phenomena existing in the contact between the idler screws and the pump case. Therefore, a redefined mechanical model based on the journal bearing theory [45] is proposed. The resulting improved mathematical model offers a better prediction of the global efficiency of the triple screw pump, despite the complex dry contact conditions induced by the pump manufacturing, representing a further modelling advancement with respect to [44].

This mathematical model has been used as a virtual tool to design a specific solution for engine thermal management. A triple screw pump was suitably designed for an IVECO F1C 3L turbocharged diesel engine widely used both for light and heavy duty applications.

This pump was investigated when operating in a homologation WLTC, and its performances were compared with those of a typical centrifugal pump matching the same mass flow rate produced by the centrifugal pump, which is considered as the reference solution. Results show that the electrically actuated triple screw pump allows a 13.8% reduction of the energy absorbed during the cycle to cool the engine, compared to the energy absorbed by the standard centrifugal pump. This reduction is due to the improved efficiency of screw pumps, which remains high even when the pump operating point varies. This behaviour is as greater as more the screw pump is designed to operate in low speed ranges.

Therefore, these results suggest that electrically actuated screw pumps properly designed for engine cooling applications may represent an efficient technical solution for engine thermal management characterized by a reduced energy absorption during the homologation WLTC. The consideration that during homologation the propulsion energy is reduced makes the energy saving requested by the pump interesting for CO_2 reduction.

2   Triple screw pump modelling

In triple-screw pumps, three rotating screws move the fluid along their axial direction from the suction to the discharge chambers, linked to the inflow and the outflow pipes,

respectively. The central screw (driver) gives the motion to the other two screws (idlers), which rotate oppositely with the same speed. The screws profiles and the pump case define the chambers in which the fluid is enclosed, whose pressure increases when they opens towards the discharge chamber.

The triple screw pump layout considered in this work has the driver screw supported by a specific bearing, which fixed its axis. Contrarily, the idler screws do not have a specific support fixing their axis, but they stay inside a cylindrical support bordered by the pump case and the driver screw. Therefore, the idlers axes can mis-align during pump operation, enabling dry contacts conditions between the idler screws and the pump case. In Fig. 1, a schematic of this type of triple screw pump is represented.
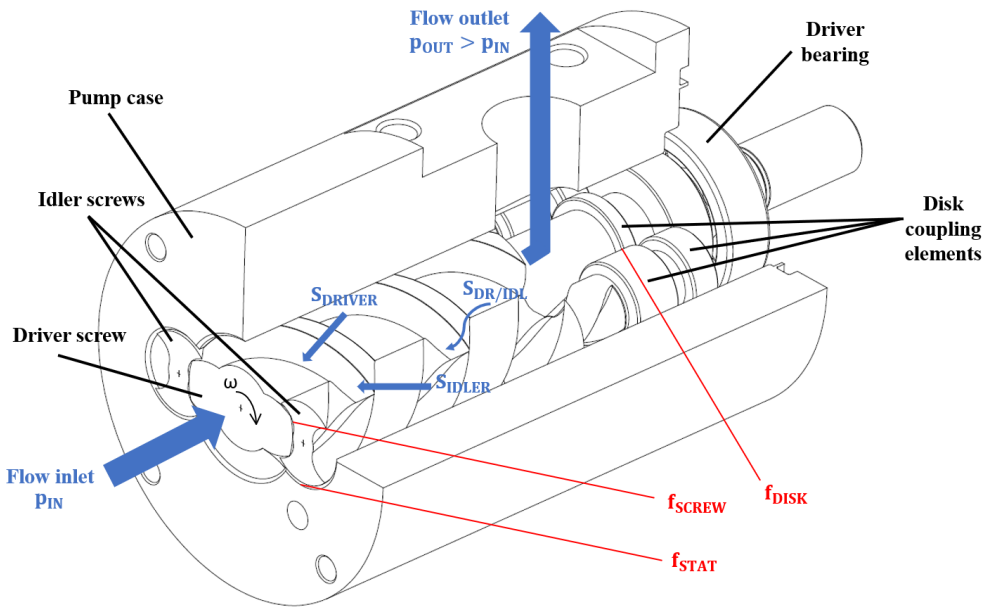

Fig. 1. Main leakage paths for the backflow inside the triple screw pump: S_{DRIVER} between the driver-screw tooth tips and the pump casing, S_{IDLER} between the idler-screw tooth tips and the pump casing, and $S_{DR/IDL}$ through the blow hole area. The driver screw is supported by a specific bearing, instead the idler screws are supported by a cylindrical housing and disk coupling elements. The friction coefficients in the contact between driver and idler screws, between idlers and pump case, and between the disk coupling elements are f_{SCREW}, f_{STAT} and f_{DISK}, respectively.

The comprehensive mathematical model of a triple screw pump characterized by this simple manufacture is presented in [44]. That model is further investigated in the present paper, developing a more accurate estimation of the power lost due to dry friction phenomena occurring inside the pump.

The model in [44] is composed by three sub-models, each of which describes the volumetric, indicated and mechanical performances of the pump, respectively (Fig. 2).
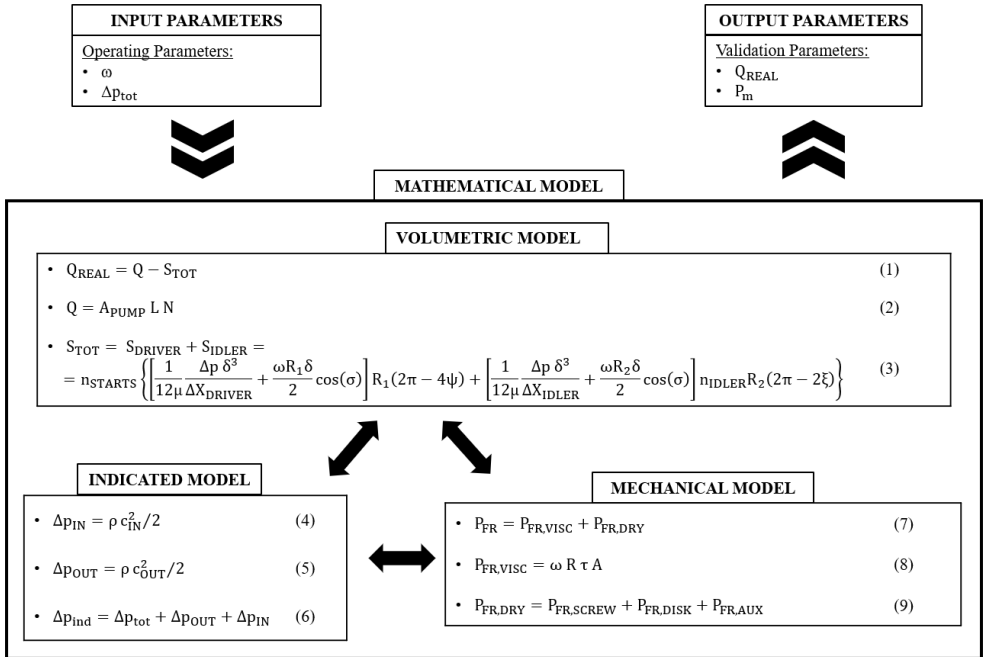
Fig. 2. Flow chart of the mathematical model of the screw pump, constituted by three sub-models: the volumetric, indicated and mechanical models.

The volumetric model calculates the backflow occurring inside the pump during its operation, due to the pressure gradient opposed to the flow motion and the existence of clearances between the screws and the pump case. Ideally, the overall backflow S_{TOT} can be divided into three different contributions, according to the clearances through which it occurs (Fig. 1): the backflow S_{DRIVER}, which occurs through the driver-case clearance, the backflow S_{IDLER}, which occurs through the idler-case clearance, and the backflow $S_{DR/IDL}$, which occurs through the driver-idler clearance, i.e. through the blow-hole line. The backflow S_{TOT} is calculated through a lumped parameter model based on a suitably redefined Poiseuille-Couette modelling. The complex geometry of the leakage flow channels has been simplified to calculate the S_{DRIVER} and S_{IDLER} contributions (Eq. 3 in Fig. 2), while the third contribution $S_{DR/IDL}$ is assumed to be negligible. Once the backflow is known, the actual flow rate Q_{REAL} (Eq. 1 in Fig. 2) is obtained by subtracting the backflow S_{TOT} to the ideal flow rate Q (Eq. 2 in Fig. 2).

The indicated performances of the pump are calculated in [44] through a lumped parameter model. This model takes into account the increased overall pressure difference acting on the screws, due to the power lost during the filling and emptying of the suction and discharge plenums, respectively. Instead, pressure spikes occurring in the fluid moving inside the chambers identified by the screws are neglected. Therefore, the indicated cycle is assumed to be composed by two isochoric and two isobars transformations: the two isobars are spaced by a pressure difference Δp_{ind} (Eq. 6 in Fig. 2) higher than the pressure difference Δp_{tot} existing between discharge and suction pipes.

The mechanical model in [44] calculates the power losses inside the pump, which can be distinguished into two contributions: viscous and dry friction losses.

As for the backflow, the viscous losses $P_{FR,VISC}$ (Eq. 8 in Fig. 2) are calculated with a lumped parameter model from the solution of the flow field given by the Poiseuille-Couette theory inside the clearances between the screw tips and the pump case.

On the other hand, the dry friction losses depend on the friction conditions realized in the mechanical couplings (Fig. 1). The driver screw is supported by an external bearing, and a lip seal avoids leakage of fluid to the outside. Instead, the idler screws are simply positioned inside a cylindrical support, without dedicated bearings and sealings for their shafts. This simple layout allows axes misalignments, and thus dry contacts between the screws themselves and with the pump case.

Therefore, the friction power losses $P_{FR,DRY}$ (Eq. 9 in Fig. 2) are calculated by summing together the friction power lost in the interactions between the screws $P_{FR,SCREW}$, in the disk coupling elements $P_{FR,DISK}$, and in the driver sealing and bearing $P_{FR,AUX}$.

Specifically, $P_{FR,SCREW}$ and $P_{FR,DISK}$ were calculated solving the equilibrium equations of the driver and idler screws: the resistant torque was calculated identifying three friction coefficients f_{STAT}, f_{SCREW} and f_{DISK} (Fig. 1), assuming them to be constant when the pump operating point varies. Instead, $P_{FR,AUX}$ was calibrated experimentally, testing the pump without mounting the idler screws.

The main limits of this model are related to the impossibility to represent correctly the effects of dry friction phenomena when the pump operating point varies. In fact, the above mentioned friction coefficients implemented in the model were assumed to be constant, neglecting their dependency with pressure head and pump speed. This simplified modelling showed its effects in the error between experimental and calculated power absorbed by the pump, which ranged between 10% and 15%, contrarily to the few percentage points error observed in the flow rate calculation.

In this paper, the mechanical model developed in [44] has been further investigated. A deeper study of the friction coefficients used to calculate the friction power losses is conducted, developing a mechanical model capable to predict the friction coefficient value when the pump operating point varies.

From journal bearing theory [45], a suitable new mechanical modeling has been developed, focusing the attention on the friction coefficient f_{STAT} between idler screws and casing. This friction coefficient has a significant importance on power losses, considerig that idler screws are simply entrained inside a cylindrical support, enabling dry friction phenomena between them and pump case for some operating points of the pump. In order to validate this critical phenomenon, a suitable experimental activity has been conducted, revealing a significant variation of f_{STAT} when a typical adimensional parameter describing the hydro-dinamically support of the idler screws varies. A significant improvement has been reached with respect to the previous model in [44] when the theoretical mechanical power is compared with the esperimental values.

3   A new friction modelling between idlers and casing and experimental validation

The mechanical model in [44] requires the definition of the friction coefficients f_{STAT}, f_{SCREW} and f_{DISK} to calculate the mechanical power absorbed by the pump: the friction coefficients f_{SCREW} and f_{DISK} are involved in the interactions between driver and idler screws, instead the friction coefficient f_{STAT} defines the contact conditions between idler screws and pump case (Fig. 1). These friction coefficients were identified by varying them within typical ranges for steel-steel contact, and assuming them to be insensitive to pump operating conditions, i.e. pump speed and pressure rise. Specifically, the values reported in Table 1 were found, in order to better match the mechanical power absorbed by the pump measured during the experimental activity.

Table 1. Friction coefficients involved in the mechanical model of the screw pump [44].

Parameter	Value	Unit
f_{STAT}	0.16	-
f_{SCREW}	0.1	-
f_{DISK}	0.1	-

In this paper, the calculation of the mechanical power absorbed by the pump has been improved introducing a more detailed mechanical model for the estimation of the friction coefficient f_{STAT}, and assuming the same values for f_{SCREW} and f_{DISK}.

In fact, the idler screws shafts are not supported by any bearings, being simply entrained inside a cylindrical support bordered by the pump case and the driver screw. This layout simplifies the pump manufacture, as generally requested by automotive applications, but enables axes misalignments, and thus occasional dry friction phenomena between idlers and casing during pump operation. Surface damages, in fact, are often found after operation and the occurrence that the fluid operated is a mixture of water and glycol (instead of being a more conventional oil for oil dynamic applications) increases the risks of damages. Therefore, a dedicate discussion about the values assumed by the friction coefficient f_{STAT} during pump operation is necessary to improve the mechanical model effectiveness.

A relation between the friction coefficient f_{STAT} and the pump operating point is developed, referring to the journal bearing theory [45].

The motion of the idler screw inside its cylindrical support can be analysed as a shaft journal rotating inside a bushing element. That mechanical coupling is described by Petroff's equation, which gives a linear relation between the coefficient of friction f and the bearing characteristic number μN/p, where μ, N and p are the dynamic viscosity of the fluid, the shaft speed and the pressure inside the lubrication film, respectively. Therefore, the bearing number defines the hydrodynamic conditions of the lubricating film supporting the shaft, which determine the friction coefficient of the journal bearing.

Similarly, the idler screw rotating inside the pump case is supported hydrodynamically by the film of fluid entrained in the clearance existing between these two elements. The flow conditions of this thin film of fluid are determined by pump speed and pressure rise. For a given pump speed, the higher is the pressure rise across the screws, the higher is the backflow occurring through the clearances between idler and casing, and thus the higher is the hydro-dynamic support of the screw. Consequently, a lower friction coefficient should be observed. Moreover, this effect should decrease for high pump speeds, because the idler screw is more subjected to the gyroscopic effect, which tends to stabilize its rotational axis. This behaviour can be expressed by equation (10) and (11), which show the friction coefficient f_{STAT} as a function of the bearing number μN/p, through a proportionality factor k(N), which is inversely proportional to the pump speed N.

$$f_{STAT} = k(N)\,\frac{\mu\,N}{p} \tag{10}$$

$$k(N) = \frac{a}{N} + b \tag{11}$$

These relations have been introduced in the mechanical model developed in [44], and the coefficients a and b in equation (11) have been identified minimizing the error between the mechanical power calculated by the model and the one measured experimentally. To this end, the experimental data used in the previous validation of the model in [44] have been considered. The obtained values of a and b are reported in Table 2.

Table 2. Parameters defining the proportionality factor k, used to calculate f_{STAT}.

Parameter	Value	Unit
a	$1.12 \cdot (10^9)$	rpm
b	$2.09 \cdot (10^5)$	-

The friction coefficients identified during the minimization process of the error in the absorbed power calculation, and the model defined by equations (10) and (11) with a and b as in Table 2, are represented as a function of the dimensionless quantity μN/p in Fig. 3. The mechanical model is a bundle of straight lines passing through the origin, with a slope decreasing with the idler screw speed, and minimum and maximum values fixed at 0.05 and 0.2, respectively. The friction coefficients optimized for each working point are arranged along these lines, confirming the validity of this modelling approach.
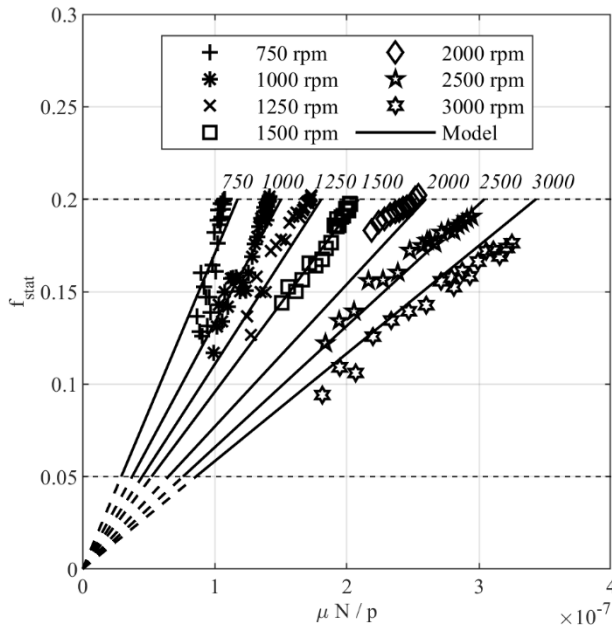

Fig. 3. Friction coefficient between idler screw and pump case f_{STAT}, as a function of the dimensionless quantity μN/p. The symbols represent the values minimizing the error in the mechanical power calculation for each working point. Instead, the lines represent the values calculated by the mechanical model.

Thus, these trends show that, for a given pump speed N, a decrease in the average pressure p of the fluid, supporting hydro-dynamically the rotating idler screw, determines an increase of the friction coefficient f_{STAT}, which has a maximum value equal to 0.2. Vice versa, an increase in the average pressure determines a decrease down to 0.05 for this friction coefficient. The physical meaning of these trends is that the higher is the pressure of the backflow fluid, passing through the clearance between the idler screw and the pump case, the more the idler screw is supported hydrodynamically by the fluid, and thus the less is the probability of dry contact conditions with the pump case, i.e. the friction coefficient f_{STAT} assumes smaller values. Therefore, these trends offer a simple modelling of the undefined

type of contact conditions realized between the unconstrained idler screws and the pump case when the pump operating point (speed and pressure) changes: contacts tending towards dry conditions are modelled with higher friction coefficients, and vice versa.

Finally, the mechanical model defined by equations (10) and (11), with a and b specified by the values reported in Table 2, allows to calculate the friction coefficient f_{STAT} between idler and casing when the pump operating point varies. The reliability of the redefined overall model of the triple screw pump has been assessed through a dedicated validation, discussed in sections 4 and 5.

4 Experimental setup

The geometry of triple screw pumps is defined by a specific set of geometrical parameters. A detailed discussion of these parameters is developed in [44]. Instead, the main geometrical features are summarized in the present paper.

The dimensions of driver and idler screws are defined by the pump series and the proportionality factor f. The pump series is a set of three numbers: the Driver Screw Outer Diameter (D_1), the Idler Screw Outer Diameter (D_2) and the Tooth Height (t). The real dimensions of D_1, D_2 and t are obtained by multiplying each number of the pump series for the scale factor f.

The axial cross section of the screws is defined by the screw angles α, β and γ, and by the ratio A_γ/R_2^2. The angles α and β define the angular extension of the teeth of driver and idler screws, respectively. They are calculated from their ratio β/α, and from the angle γ. The angle γ defines the angular extension of the epicycloid profile, which links inner and outer diameters of each screw. It is calculated imposing the maximum meshing angle condition [44], once the outer diameters of the screws (D_1 and D_2) and the tooth height (t) are known. The ratio A_γ/R_2^2 takes into account of a slight approximation in the idler cross sectional area calculation. Its value depends on the specific pump series.

The axial length of the screws is defined by the winding angle of the screws teeth σ and the number of stages n_{STAGE}. This latter parameter defines the number of axial repetition of a stage, that is a complete axial revolution of the screws teeth.

Further parameters defining the screw pump layout are the number of starts n_{STARTS}, which defines the number of teeth of each screw, and the number of idler screws n_{IDLER}, equal to two in this analysis. Finally, the clearances between the screws and the pump case are defined by δ_{DRIVER} and δ_{IDLER}, for driver and idler screws respectively.

In this paper, a triple screw pump of the 5-3-1 series is considered for the validation of the model. It has a proportionality factor equal to 8 and a number of stages equal to 1.31, which determine a 48 cm^3 displacement, and external diameters of driver and idler screws equal to 40 mm and 24 mm, respectively. The working fluid adopted during the experimental campaign is a 50% glycol-water-mixture. The main geometrical parameters of this triple screw pump are summarized in Table 3.

Table 3. Main geometrical parameters of the triple screw pump considered for the validation of the model.

Parameter	Value	Unit
Series	5-3-1	-
f	8	-
n_{STAGE}	1,31	-
n_{STARTS}	2	-

σ	61,4	deg
β/α	2,65	-
A_γ / R_2^2	0,0265	For 5-3-1 series
n_{IDLER}	2	-
δ_{DRIVER}	120	μm
δ_{IDLER}	10	μm
Displacement	48	cm^3
$D_{SUCTION}$	24	mm
$D_{DISCHARGE}$	24	mm

The experimental campaign necessary to validate the overall mathematical model of the triple screw pump was conducted using the test bench developed in [46]: its layout is represented in Fig. 4, and the uncertainties of its measuring devices are reported in Table 4. The hydraulic head to the pump is given by a 24 litres pressurized tank, whose pressure level is increased using compressed air: this is necessary to prevent cavitation phenomena during pump operation. The pressure drop across the pump is set by regulating a pneumatic proportional valve. Pressure is measured across the pump through diaphragm pressure sensors, and the flow rate is measured by a turbine flowmeter.

A three-phase electric motor driven by an inverter moves the pump. Torque and speed are evaluated through a torque meter: this enables to calculate the overall mechanical efficiency of the pump. Finally, input and output signals are managed in a data acquisition and control unit (DAQ).
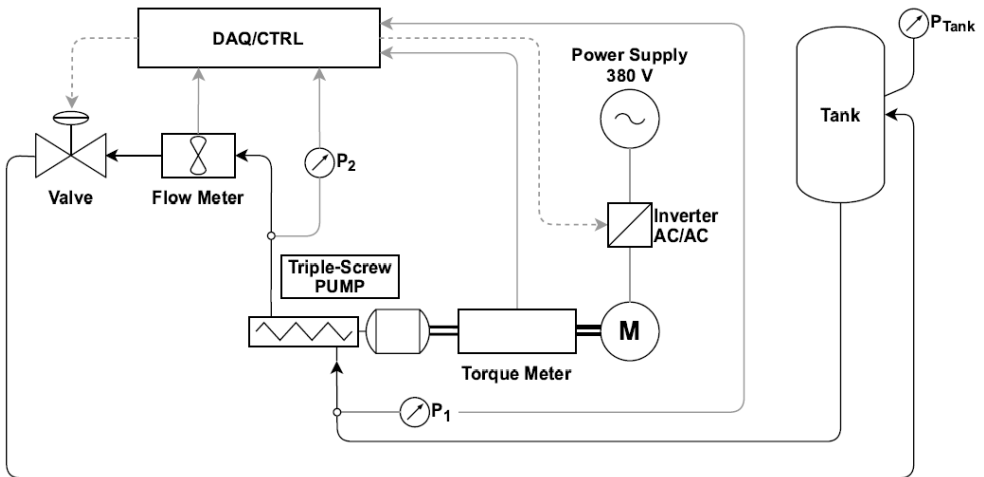

Fig. 4. Layout of the dynamic test bench.

Table 4. Uncertainties of the measuring devices.

Physical quantity	Uncertainty
Torque	0.015 Nm
Velocity	0.01 %
Flow rate	0.15 %

Pressure	0.003 bar
Pressure rise	< 1.5 %
Mechanical power	< 7%

5   Pump performances validation

The model was validated considering a wide experimental campaign developed with the experimental setup described in section 4. The pump speed was varied between 750 rpm and 3000 rpm, and the hydraulic permeability of the circuit was varied to reach a pressure rise across the pump up to 3 bar. In these conditions, the screw pump delivers a flow rate ranging between 30 l/min and 140 l/min, absorbing up to 970 W at 3000 rpm.

The validation is realized by comparing the flow rate Q_{REAL} and the absorbed mechanical power P_m calculated by the model, with the corresponding measured values, giving as inputs the measured values of pump speed ω and overall pressure rise Δp.

As expected, the flow rate Q_{REAL} is calculated with a mean error of the same order of magnitude obtained in [44], being unchanged the volumetric model of the triple screw pump.

On the other hand, the mechanical power absorbed by the pump P_m is calculated with a mean error equal to 6.1%, and a standard deviation equal to 7.4%. This result shows the benefits obtained considering the friction coefficient between idler screws and pump case f_{STAT} variable with pump speed and output pressure. In fact, in [44] the mean error in the mechanical power calculation was 13.5%, with a standard deviation of the same order of magnitude. Therefore, the mechanical model developed in the present paper allows a reduction of the error close to 50% with respect to the previous simpler model. Moreover, the uncertainty of the measured mechanical power must be considered: in fact, it is equal to 7% (Table 4) due to the absolute uncertainty in the torque measure. This testifies a significant dispersion of data, due to operating issues experienced during tests (high revolution speeds, no lubrication, low pressurization).

The global efficiency can be observed in Fig. 5. The pump model shows a good agreement with experimental values, and the real trends are reproduced correctly. Moreover, it is important to observe the maximum global efficiency reached by this pump, about 70% at 1500 rpm and 2.5 bar, and its slight variation when the operating point of the pump varies. These data are unreachable with a centrifugal pump.
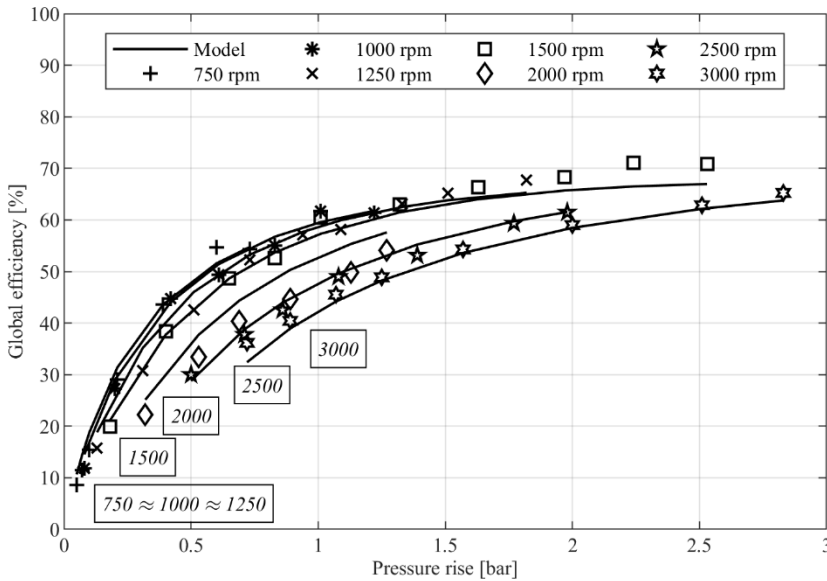
Fig. 5. Global efficiency, as a function of pressure rise, calculated by the model (continuous lines), and by the measured values (symbols), varying the pump speed from 750 to 3000 rpm.

6 Engine cooling application

The aim of the present paper is to compare the performances of a triple screw pump electrically actuated with those of a typical centrifugal pump, when operating in a WLTC with the same engine cooling circuit.

This study moves from the observation that screw pumps efficiency is less dependent on rotational speed and pressure head compared to centrifugal pumps efficiency. This aspect has been observed also for the triple screw pump tested in this work to validate the model (Fig. 5): the overall efficiency of the screw pump ranges between 50% and 70%, which are unconventional values for the specific sector. Moreover, low pump speeds allow to reach higher values of efficiency, which remains almost constant for a wide range of pressure heads: therefore, for a given automotive application, the screw pump geometry should be chosen in order to keep the pump speed as low as possible.

In this paper, an IVECO F1C diesel engine for a light duty application is considered [47], assuming the permeability curves reported in Fig. 6, corresponding to closed and open thermostat configurations, respectively.
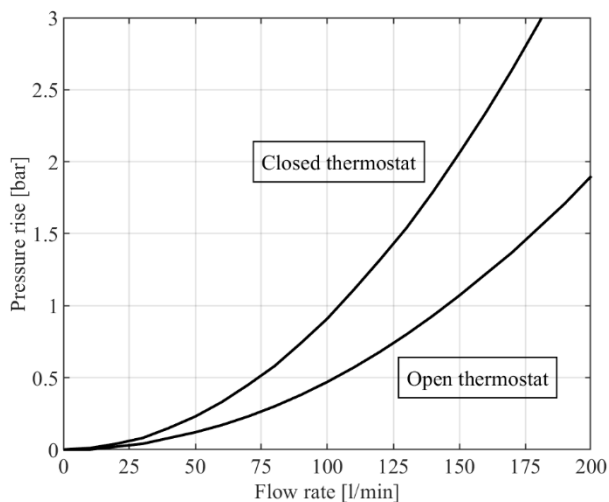
Fig. 6. Permeability curves of the diesel engine cooling circuit.

The original system adopts a centrifugal pump mechanically linked with the crankshaft. This pump is designed to deliver 240 l/min and 2.8 bar at 4000 rpm of engine speed, with a maximum efficiency equal to 46%, i.e. the BEP – Best Efficiency Point.

In order to investigate the screw pump performances for this engine cooling application, the mathematical model developed in sections 2 and 3 has been utilized to design a specific pump for the IVECO F1C engine. The output of the design was a screw pump with the same geometric proportions as those reported in Table 3, but with a 50% increase of its displacement (from 48 cm^3 to 72 cm^3). This displacement was identified in order to keep the revolution speed of the pump lower than 3500 RPM. This maximum value is reached when the flow rate approaches 240 l/min, which is the flow rate at BEP for the centrifugal pump.

Moreover, the triple screw pump was assumed to be actuated by an electric motor, with an average electric efficiency equal to 0.9: this allows to vary the pump speed independently from the crankshaft, delivering the right amount of flow rate requested by the engine during the WLTC, that is the flow rate delivered by the centrifugal pump.

Therefore, the performances of the centrifugal pump and of the electrically actuated triple screw pump are presented from Fig. 7 to Fig. 10.

The speed profiles of the two pumps during the WLTC are compared in Fig. 7. The electric screw pump follows its own path, being disengaged from the crankshaft speed and simultaneously regulated to satisfy the engine cooling requirements, which coincide with the flow rate delivered by the centrifugal pump (Fig. 8). This was calculated knowing the hydraulic characteristics of the circuit (with the thermostat opened or closed, Fig. 6) and the revolution speed of the pump which is mechanically linked to the engine crankshaft. The sequence of the crankshaft speeds during the homologation WLTC was calculated when the sequence of the operating points of the engine running the cited cycle was known. The mean speed of the centrifugal pump during most of the cycle is about 2500 rpm, while the corresponding value of the electric triple screw pump is about 1250 rpm. This allows to deliver about 90 l/min of flow rate, which varies during the cycle from a minimum of 27 l/min to a maximum of 195 l/min.
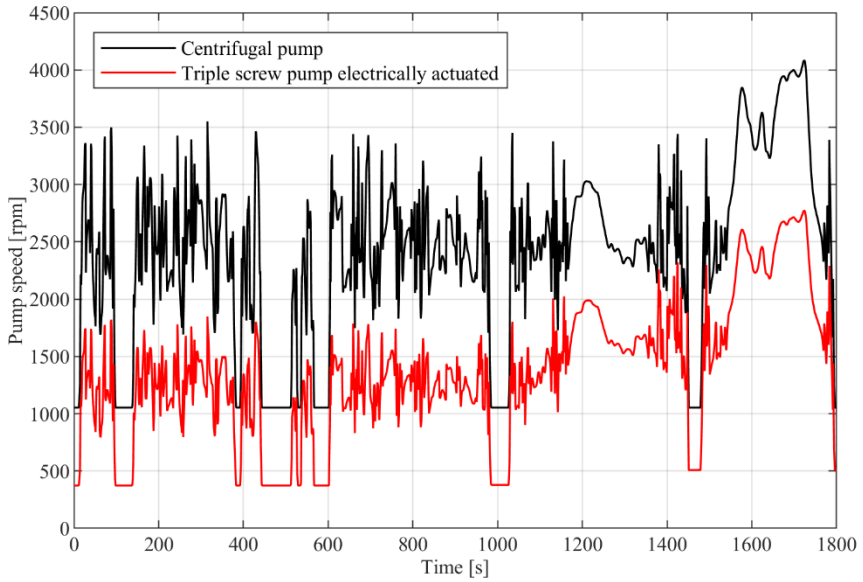
Fig. 7. Speed of the centrifugal pump during a WLTC, compared with that of the electrically actuated triple screw pump.
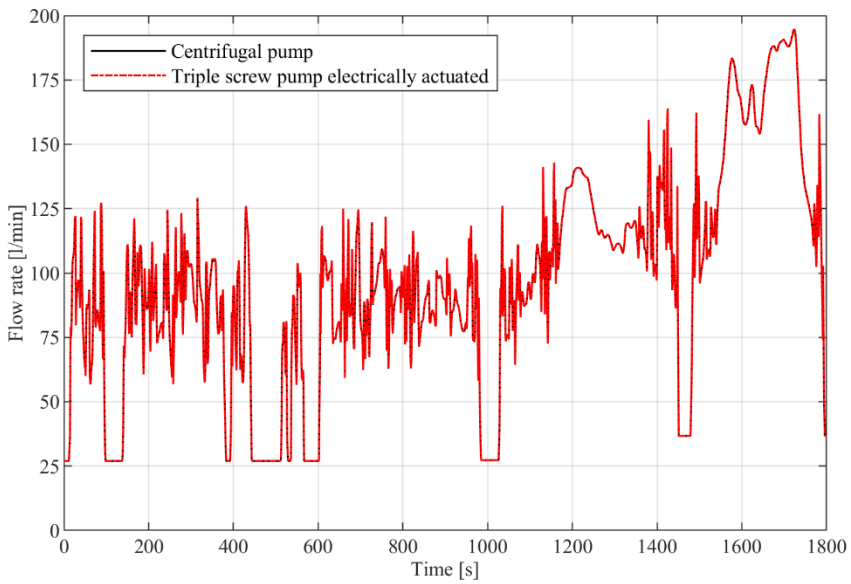
Fig. 8. Flow rate delivered by the centrifugal pump during a WLTC, compared with that of the electrically actuated triple screw pump. The two curves are substantially coincident.

14

The global efficiency of the centrifugal pump is compared with that of the electrically actuated triple screw pump in Fig. 9. The efficiency of the electric screw pump takes into account also the efficiency of the electric motor, which is assumed constant during the cycle and equal to 0.9. The electrical screw pump shows a higher global efficiency than that of the centrifugal pump, although this advantage is progressively reduced after the thermostat valve opening, which happens at about 1200 s.

This is due to the lower efficiency of the electric screw pump when it operates with higher pump speeds, which are reached in the second part of the cycle, after the thermostat valve opening. Instead, the centrifugal pump increases its efficiency after 1200 s, because it moves towards operating points with high flow rate, closer to its BEP.
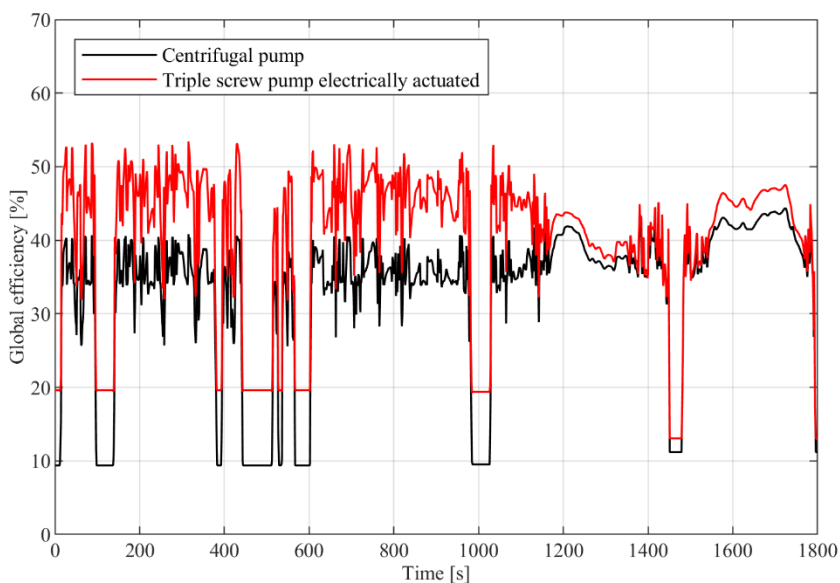

Fig. 9. Global efficiency of the centrifugal pump during a WLTC, compared with that of the electrically actuated triple screw pump.

The cumulative energy absorbed by the two pumps during the cycle is reported in Fig. 10. The electric triple screw pump aborbes 562 kJ of cumulated energy during the WLTC, against 652 kJ absorbed by the traditional centrifugal pump, leading to a 13.8% reduction of energy requested by the pump to cool the engine. This result is due to the improved efficiency of the triple screw pump, which keeps higher values even when the pump speed varies, despite the adverse effect on the global efficiency introduced by the electric drive. Even greater energy savings could be achieved if the displacement of the volumetric pump is further increased, resulting for a given flow rate to be delivered in a lower revolution speed, which always increases the efficiency of the volumetric pump. Considering that this displacement increase produces a dimension increase too, a trade-off between space availability for the pump and efficiency, so energy reduction, could be done.
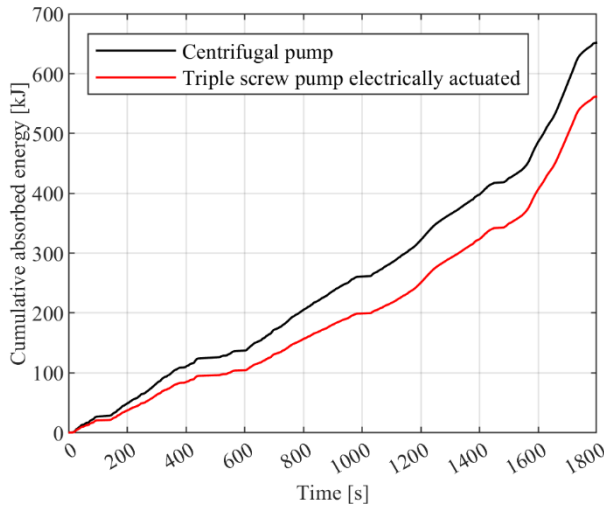
Fig. 10. Cumulative energy absorbed by the centrifugal pump during a WLTC, compared with that of the electrically actuated triple screw pump.

7   Conclusions

The aim of this paper is to evaluate the performances of triple screw pumps when operating as an alternative to the more conventional centrifugal pumps in the cooling circuit of ICEs. In fact, screw pumps are volumetric-type machines, and so they keep high efficiencies even when the pump speed varies. This feature is particularly useful in automotive or ligh duty applications, where the continuous variation of the engine working point imposes a continuously variable pump speed.

To this end, the lumped parameter model of a triple screw pump developed in [44] has been further investigated. Specifically, a more refined mechanical model has been developed and experimentally validated, to reduce the error in the mechanical power calculation. In fact, the model was built for a particularly simple pump layout, being cheap and reliable manufacturing solutions requested in the automotive sector. The pump, in fact, has only one bearing supporting the driver screw, and two cylindrical supports for the idler screws, without any bearings fixing their axes. Misalignments of the screw axes certainly occur, and consequently dry friction phenomena; both increase the complexity of the prediction of the mechanical power absorbed by the pump.

The paper presents a model for the dry friction by adapting the journal bearing theory to this specific pump manufacture and validates it with an extensive experimental champain. It was inserted in a comprehensive 0-D pump model refining the global efficiency prediction. In fact, the mechanical power is calculated with a mean absolute error equal to 6.1%, more than halved compared to the value obtained in [44].

Subsequently, the mathematical model has been used to design a triple screw pump for an IVECO F1C engine. This screw pump has been studied when operating as the cooling pump during a WLTC, and its performances have been compared to those of the standard centrifugal pump used in that engine. Moreover, the triple screw pump has been considered actuated by an electric motor, assuming a mean electric efficiency equal to 0.9. This allows to deliver the same flow rate delivered by the centrifugal pump during the cycle.

Results show that the electrically actuated triple screw pump allows to reduce the overall absorbed energy of about 13.8% compared to the centrifugal pump. This result is due to the

capability of screw pumps to keep high efficiencies when the pump operating point varies. This behaviour is as greater as more the screw pump is designed to operate with lower speed ranges.

Therefore, the use of the screw pump for engine cooling applications leads to a reduction of the energy required to drive the pump over a WLTC, with lower corresponding CO_2 emissions. Moreover, an optimum thermal management of the engine can be implemented, being the flow rate delivered stricly proportional to the revolution speed and independent from the hydraulic permeability of the cooling circuit.

Acknowledgments

Nomenclature

Table of symbols			
ICE:	Internal Combustion Engine	$D_{SUCTION}$:	Diameter of the suction pipe
CFD:	Computation Fluid Dynamics	$D_{DISCHARGE}$:	Diameter of the discharge pipe
WLTC:	Worldwide Harmonized Light Vehicles Test Cycle	N, ω:	Rotation speed
BEP:	Best Efficiency Point	Q:	Theoretical flow rate
f:	Scale factor	S_{DRIVER}:	Backflow across driver-screw tooth tips and pump casing
D_1:	Outer diameter of the driver screw	S_{IDLER}:	Backflow across idler-screw tooth tips and pump casing
D_2:	Outer diameter of the idler screw	$S_{DR/IDL}$:	Backflow across contact regions between the screws
d_1:	Inner diameter of the driver screw	S_{TOT}:	Overall backflow
d_2:	Inner diameter of the idler screw	Q_{REAL}:	Effective flow rate
t:	Tooth height	Δp_{TOT}:	Discharge-suction pressure differential
α:	Angle of outer radius of driver screw tooth	Δp_{IND}:	Outlet-inlet pressure differential
β:	Angle of outer radius of idler screw tooth	τ:	Shear stress of the fluid in contact with the screw
γ:	Epicycloid angle	A:	Action area of the fluid shear stress
ψ:	Maximum meshing angle of the driver screw	P_t:	Theoretical power output
ξ:	Maximum meshing angle of the idler screw	P_i:	Indicated power
σ:	Screw angle	P_h:	Hydraulic power

n_{STAGE}:	Number of stages of the pump	P_m:	Mechanical power
n_{START}:	Number of screws starts	P_{FR}:	Friction power losses
n_{IDLER}:	Number of idler screws	η_v:	Volumetric efficiency
$n_{CHAMBERS}$:	Number of sealing chambers	η_i:	Indicated efficiency
δ_{DRIVER}:	Clearance between the driver screw and the stator	η_m:	Mechanical efficiency
δ_{IDLER}:	Clearance between the idler screw and the stator	η_g:	Global efficiency
δ:	Equivalent clearance for the backflow calculation	μ:	Dynamic viscosity of the fluid
A_γ:	Epicycloid Area	ρ_{FLUID}:	Density of the fluid
A_{PUMP}:	Flow area of the screw pump	ρ_{IDLER}:	Density of the idler screw material
A_{CASE}:	Cross sectional area of the pump case	f_{SCREW}:	Friction coefficient between the idler and the driver screws
A_{DRIVER}:	Cross sectional area of the driver screw	f_{STAT}:	Friction coefficient between the idler screw and the stator
A_{IDLER}:	Cross sectional area of the idler screw	f_{DISK}:	Friction coefficient between the disk coupling elements
L:	Screw pitch length		

References

1. European Parliament, Regulation (EU) No 333/2014, Off. J. of the Eur. Un. (2014).
2. European Parliament, Regulation (EU) No 253/2014, Off. J. of the Eur. Un. (2014).
3. EEA, Annual European Union greenhouse gas inventory 1990 – 2019 and inventory report 2021, (2021).
4. IEA, Global EV Outlook 2021, (2021).
5. S.I. Ehrenberger, M. Konrad, F. Philipps, Pollutant emissions analysis of three plug-in hybrid electric vehicles using different modes of operation and driving conditions, Atmos. Environ. **234** (2020) 117612. https://doi.org/10.1016/j.atmosenv.2020.117612.
6. N. Rietmann, B. Hügler, T. Lieven, Forecasting the trajectory of electric vehicle sales and the consequences for worldwide CO_2 emissions, J. Clean. Prod. **261** (2020) 121038. https://doi.org/10.1016/j.jclepro.2020.121038.
7. G. Zheng, Z. Peng, Life Cycle Assessment (LCA) of BEV's environmental benefits for meeting the challenge of ICExit (Internal Combustion Engine Exit), En. Rep. **7** (2021) 1203–1216. https://doi.org/10.1016/j.egyr.2021.02.039.
8. J. Gao, G. Tian, A. Sorniotti, A. E. Karci, R. Di Palo, Review of thermal management of catalytic converters to decrease engine emissions during cold start and warm up, Applied Thermal Engineering 147 (2019) **177–187**, https://doi.org/10.1016/j.applthermaleng.2018.10.037.

9. D. Di Battista, D. Vittorini, F. Fatigati, R. Cipollone, Technical review of opportunities to reduce the warm-up time of lubricant oil in a light-duty diesel engine, AIP Conference Proceedings **2191**, 020065 (2019), https://doi.org/10.1063/1.5138798.

10. D. Vittorini, D. Di Battista, R. Cipollone, Engine oil warm-up through heat recovery on exhaust gases – Emissions reduction assessment during homologation cycles, Therm. Sc. and Eng. Progr. **5** (2018) 412–421, https://doi.org/10.1016/j.tsep.2018.01.010.

11. R. Cipollone, D. Di Battista, A. Gualtieri, A novel engine cooling system with two circuits operating at different temperatures, Energy Conversion and Management, 75, pp. **581-592**, (2013), http://dx.doi.org/10.1016/j.enconman.2013.07.010.

12. H. Chen et al., FCA US LLC, Chiller system for an engine with a forced induction system, United States Patent, US 10006339B2, (2018).

13. D. E. Hornback et al., FCA US LLC, Vehicle thermal system for reduced fuel consumption, United States Patent, US 10216258B1, (2019).

14. D. Di Battista, R. Cipollone, High efficiency air conditioning model based analysis for the automotive sector, International Journal of Refrigeration, 64, pp. **108-122**, (2016), http://dx.doi.org/10.1016/j.ijrefrig.2015.12.014.

15. R. Cipollone, D. Di Battista, A. Gualtieri, Head and block split cooling in ICE, IFAC Proceedings Volumes (IFAC-PapersOnline), 45 (30), pp. **400-407**, (2012), https://doi.org/10.3182/20121023-3-FR-4025.00056.

16. T. Castiglione, P. Morrone, L. Falbo, D. Perrone, S. Bova, Application of a model-based controller for improving internal combustion engines fuel economy, Energies, 13 (5), art. no. **1148**, (2020), https://doi.org/10.3390/en13051148.

17. A. K. Haghighat, S. Roumi, N. Madani , D. Bahmanpour, M. G. Olsen, An intelligent cooling system and control model for improved engine thermal management, Applied Thermal Engineering 128 (2018) **253–263**, http://dx.doi.org/10.1016/j.applthermaleng.2017.08.102.

18. H. Mu, Y. Wang, H. Teng, Y. Jin, X. Zhao, X. Zhang, Cooling system based on double-ball motor control valve, Advances in Mechanical Engineering, Vol. **13(5) 1–12** (2021), https://doi.org/10.1177/16878140211011280.

19. L. Mariani, M. Di Bartolomeo, D. Di Battista, R. Cipollone, F. Fremondi, R. Roveglia, Experimental and numerical analyses to improve the design of engine coolant pumps, E3S Web of Conf. **197**, 06017 (2020), https://doi.org/10.1051/e3sconf/202019706017.

20. R. Cipollone, D. Di Battista, G. Contaldi, S. Murgia, M. Mauriello, Development of a sliding vane rotary pump for engine cooling, Energy Procedia **81** (2015) 775–783. https://doi.org/10.1016/j.egypro.2015.12.083.

21. R. Cipollone, G. Bianchi, D. Di Battista, F. Fatigati, Fuel economy benefits of a new engine cooling pump based on sliding vane technology with variable eccentricity, Energy Procedia **82** (2015) 265–272. https://doi.org/10.1016/j.egypro.2015.12.032.

22. R. Cipollone, D. Di Battista, Sliding vane rotary pump in engine cooling system for automotive sector, Appl. Therm. Eng. **76** (2015) 157–166. https://doi.org/10.1016/j.applthermaleng.2014.11.001.

23. G. Bianchi, F. Fatigati, S. Murgia, R. Cipollone, Design and analysis of a sliding vane pump for waste heat to power conversion systems using organic fluids, Appl. Therm. Eng. **124** (2017) 1038–1048. https://doi.org/10.1016/j.applthermaleng.2017.06.083.

24. N. Stosic, I. Smith, A. Kovacevic, E. Mujic, Review of Mathematical Models in Performance Calculation of Screw Compressors, International Journal of Fluid Machinery and Systems, **Vol.4, No.2**, April-June, (2011), DOI: 10.5293/IJFMS.2011.4.2.200.

25. I.K. Smith, N. Stosic, A. Kovacevic, Power Recovery from Low Grade Heat by Means of Screw Expanders, Woodhead Publishing, (2014), ISBN 978-1-78242-189-4.

26. Z. Wang, H. Wang, J. Wang, Q. Li, Q. Feng, Theoretical study on wear characteristics of single screw refrigeration compressor with multicolumn envelope meshing pair, International Journal of Refrigeration 102 (2019) **1–11**, https://doi.org/10.1016/j.ijrefrig.2019.03.004.

27. D. Ziviani, E. A. Groll, J. E. Braun, M. De Paepe, Review and update on the geometry modeling of single-screw machines with emphasis on expanders, International Journal of Refrigeration 92 (2018) **10–26**, https://doi.org/10.1016/j.ijrefrig.2018.05.029.

28. I. J. Karassik, J. P. Messina, P. Cooper, C. C. Heald, Pump Handbook, 3rd Edition, McGraw-Hill, (2001).

29. P. Dong, S. Zhao, Y. Zhao, P. Zhang, Y. Wang, Design and experimental analysis of end face profile of tri-screw pump, Institution of Mechanical Engineers Part A, (2019), DOI: 10.1177/0957650919870373.

30. J. Xu, Q. Feng, W. Wu, Geometrical design and investigation of a new profile of the three screw pump, J. Mech. Des. Trans. ASME. 133 (2011) **1–5**. https://doi.org/10.1115/1.4004588.

31. Q. Tang, Y. Zhang, Screw optimization for performance enhancement of a twin-screw pump, Proc. Inst. Mech. Eng. Part E J. Process Mech. Eng. 228 (2014) **73–84**. https://doi.org/10.1177/0954408913478602.

32. E. Mujic, A. Kovacevic, N. Stosic, I. Smith, Advanced Design Environment for Screw Machines, Int. Compress. Eng. Conf., (2010).

33. Y. Lu, A. Kovacevic, M. Read, N. Basha, Numerical Study of Customised Mesh for Twin Screw Vacuum Pumps, Designs, 3(4), **52**, (2019), https://doi.org/10.3390/designs3040052.

34. D. Yan, A. Kovacevic, Q. Tang, S. Rane, Numerical investigation of cavitation in twin-screw pumps, Institution of Mechanical Engineers Part C, (2017), DOI: 10.1177/0954406217740927.

35. A. Putira, Parametrization of Triple Screw Pumps for Aerospace Applications, (2018), https://commons.erau.edu/edt.

36. H. Schlichting, K. Gerten, Boundary-Layer Theory, Ninth Edit, Springer, (2017), https://doi.org/10.1108/eb029898.

37. G.C. Mimmi, P.E. Pennacchi, Design of three-screw positive displacement rotary pumps, Trans. Eng. Sci. **7**, (1995).

38. G.C. Mimmi, P.E. Pennacchi, Computation of pressure loads in three screw pump rotors, J. Mech. Des. Trans. ASME, 120 (1998), **581–588**, https://doi.org/10.1115/1.2829318.

39. G.C. Mimmi, P.E. Pennacchi, Dynamic effects of pressure loads in three screw pump rotors, J. Mech. Des. Trans. ASME, 12, (1998) **589–592**, https://doi.org/10.1115/1.2829319.

40. C. Feng, P. Yueyuan, X. Ziwen, S. Pengcheng, Thermodynamic performance simulation of a twin-screw multiphase pump, Proc. Inst. Mech. Eng. Part E J. Process Mech. Eng. 215 (2001), **157–163**. https://doi.org/10.1243/0954408011530406.

41. K. Räbiger, Fluid dynamic and thermodynamic modelling of multiphase screw pumps, operating on the threshold of an exclusive gas compression, 7th International Conference on Compressors and their Systems 2011, Pages **385-400**, (2011), https://doi.org/10.1533/9780857095350.8.385.

42. D. Li, Z. He, C. Wang, Y. Guo, W. Wei, D. Lin, Z. Xing, Design methodology and performance analysis of conical rotors for dry screw vacuum pumps, Vacuum, (2021), https://doi.org/10.1016/j.vacuum.2020.110025.

43. J. Wang, F. Cui, S. Wei, R. Sha, H. Liu, Study on a novel screw rotor with variable cross-section profiles for twin-screw vacuum pumps, Vacuum, (2017), http://dx.doi.org/10.1016/j.vacuum.2017.09.006.

44. G. Di Giovine, L. Mariani, D. Di Battista, R. Cipollone, F. Fremondi, Modeling and experimental validation of a triple-screw pump for internal combustion engine cooling, Applied Thermal Engineering, (2021, under review available as private publication).

45. R. G. Budynas, J. Keith Nisbett, Shigley's Mechanical Engineering Design, 9th Edition, McGraw-Hill, (2011).

46. M. Di Bartolomeo, F. Fatigati, D. Di Battista, R. Cipollone, A New Approach for Designing and Testing Engine Coolant Pump Electrically Actuated, SAE Technical Paper 2020-01-1161, (2020), doi:10.4271/2020-01-1161.

47. D. Di Battista, R. Cipollone, Experimental and numerical assessment of methods to reduce warm up time of engine lubricant oil, Applied Energy 162 (2016) **570–580**, http://dx.doi.org/10.1016/j.apenergy.2015.10.127.